Geofísica Internacional (2025) **64-3**: 1593 - 1609

Focal mechanisms and tectonic stress field in the Valley of Mexico from local seismicity

Delia I. Bello-Segura[1], Luis Quintanar[2]* and S. K. Singh[2]

Abstract

We performed a comprehensive analysis of the seismic activity in the Valley of Mexico using the records of nearby seismic stations. Events with a high signal-to-noise ratio were chosen, i.e., where the P and S arrivals were sufficiently clear to be distinguishable. Focal mechanisms were obtained for 24 local earthquakes by means of moment tensor inversion using the ISOLA and INVERS2 software packages, finding that most of the seismicity of the Mexico Basin presents normal and strike-slip faulting. Based on the distribution of seismicity within the Valley of Mexico, we identified five areas where the activity is concentrated: Sierra de las Cruces, Central area, Southeastern area, Lake-bed area, and Sierra Chichinautzin. After carrying out a stress field inversion in each region, we found a predominantly extensional tectonic regime with small strike-slip components.. In general, the stress field found is not homogeneous over all areas, indicating complexity in the characteristics and distribution of faulting types. This complexity could be the manifestation of the transtensional stress field in the central part of the Trans-Mexican Volcanic Belt because of the oblique direction of this geological feature relative to the Middle America Trench.

Key words: Seismicity in Mexico City, Seismic Moment Tensor Inversion, Local Stress Field.

Resumen

Realizamos un análisis exhaustivo de la actividad sísmica en el Valle de México utilizando los registros de las estaciones sísmicas cercanas. Se eligieron eventos con una alta relación señal-ruido, es decir, con llegadas P y S lo suficientemente claras para ser distinguidas. Se obtuvieron mecanismos focales para 24 sismos mediante la inversión del Tensor de Momento Sísmico utilizando los métodos ISOLA e INVERS2, encontrando que la mayor parte de la sismicidad de la Cuenca de México presenta fallamiento normal y de deslizamiento de rumbo. Con base en la distribución de la sismicidad en el Valle de México, identificamos cinco áreas donde se concentra la actividad: Sierra de las Cruces, Área Central, Área Sureste, Área del lecho del lago y Sierra Chichinautzin. Después de realizar una inversión del campo de esfuerzos de cada región, encontramos un régimen tectónico dominante extensional con una pequeña componente de deslizamiento de rumbo. En general, el campo de esfuerzos encontrado no es homogéneo a lo largo de todas las zonas, lo que indica una complejidad en las características y distribución del fallamiento. Esta complejidad podría ser la manifestación del campo de esfuerzos transtensional en la parte central del Cinturón Volcánico Transmexicano debido a la dirección oblicua de este rasgo geológico con respecto a la Trinchera Mesoamericana.

Palabras clave: Sismicidad en la Ciudad de México, Inversión del Tensor de Momento Sísmico, Campo de esfuerzos local.

Received: January 6, 2025; Accepted: May 19, 2025; Published on-line: July 1, 2025.

Editorial responsibility: Dr. Roberto Ortega-Ruiz

* Corresponding author: Luis Quintanar, luisq@igeofisica.unam.mx
[1] Universidad Nacional Autónoma de México, Posgrado en Ciencias de la Tierra, Mexico City, México,
[2] Universidad Nacional Autónoma de México, Instituto de Geofísica, Mexico City, Mexico.

Delia I. Bello-Segura, Luis Quintanar, S. K. Singh

https://doi.org/10.22201/igeof.2954436xe.2025.64.3.1853

1. Introduction

Most of Mexican territory is located on the North American plate and just Baja California peninsula is located on the Pacific plate. The Cocos plate subducts beneath North American plate along 1300 km on the coast of the Pacific Ocean. Large earthquakes recorded in the Valley of Mexico are due to the subduction of these two plates. Earthquakes along this subduction zone can be intraplate or interplate, with the former occurring far from the trench. Interplate earthquakes occur at the contact between the subducting and the overriding plate.

The Basin of Mexico, the most populated region of Mexico, is in the central part of the Trans-Mexican Volcanic Belt (TMVB). This region (Figure 1) is a continental arc resulting from the subduction of the Rivera and Cocos plates beneath the North American plate. The main volcanic activity occurred during the Pliocene and Quaternary periods (Arce *et al.*, 2019). Although the Mexico basin and the Valley of Mexico may technically refer to distinct areas, here we will use the terms interchangeably; Mexico City is situated within the basin.

Except for a few cases of isolated events, the lack of data has hampered stress characterization of the Basin of Mexico in the past. Rapid increase in the instrumentation of the Valley of Mexico in recent years (Quintanar *et al.*, 2018) now allows reliable and quantitative studies of the seismicity in the region.

Historically, earthquakes have occurred in the Valley of Mexico, and some have caused damage to structures. For example, in the year 1475, before the arrival of the Spaniards, an earthquake with high intensity occurred, possibly with epicenter in the Valley of Mexico, which caused extensive damage on the constructions (García Acosta and Suárez, 1996). With the increase in seismological instrumentation in the Valley of Mexico, a relatively high level of seismic activity was determined, of small magnitude until now. However, we cannot rule out the possibility of a larger magnitude event.

In this study, we have obtained the source geometry of well recorded earthquakes in the Mexico Basin by inverting the seismic Moment Tensor. The events are grouped in five regions on the basis of their location in the valley. The stress field is calculated for each region from the inversion of focal mechanisms. We find that the results are consistent with previous works on focal mechanism determination in central Mexico (e.g. UNAM and CENAPRED Seismology Group, 1995; Arce *et al.*, 2019).

2. Geological setting

2.1 Tectonics of the Valley of Mexico

The TMVB is the largest Neogene volcanic arc in North America, with an area of 160,000 km^2 and a length of nearly 1000 km between 18°30′ and 21°30′ N in central Mexico. The basin of Mexico is a closed watershed located in the central-eastern portion of the TMVB (Ferrari *et al.*, 2012; Gómez-Tuena *et al.*, 2007). This basin has an area of ∼9540 km^2 and the lacustrine central plain has an elevation of ∼2240 m above sea level (Lugo-Hubp *et al.*, 2019), which is bounded by four volcanic Sierras: Chichinautzin, Pachuca-Tezontlalpan, Las Cruces, and Nevada to the south, north, west, and east, respectively (De Cserna *et al.*, 1987; Macías *et al.*, 2012). It also includes volcanic complexes like the Sierra Guadalupe and the Sierra Santa Catarina (García-Palomo *et al.*, 2008; Siebe and Macías, 2004). In general, the filling of the basin consists of lacustrine deposits in the upper part, and lava flows, epiclastic materials, and pyroclastic deposits at the bottom (Perez Cruz, 1988). The Valley of Mexico is located in the southern part of the Mexico basin and corresponds approximately to the area limited by 19°00′-19°45′ N and 98°45′-99°20′ W (Figure 1). Its northern limit is the town of Otumba and the ruins of the ancient settlement of Teotihuacán, to the south it is bounded by the Sierra Chichinautzin, to the west by the Sierra de las Cruces, and to the east by the Nevada range and the former Texcoco lake. It has an area of nearly 3700 km^2.

The Mexico basin is located in the central TMVB. It is surrounded by volcanic ranges of andesitic and dacitic composition (Arce *et al.*, 2019). Normal faults trending east-west and northeast-southwest have been mapped in the region. Geological and tectonic studies have been conducted for years to study the faults within the Mexico basin, some of which are active and may cause local seismicity. The map in Figure 1 shows the different fault systems in the Mexico basin.

2.2 Geotechnical zonification of Valley of Mexico

Based on the geotechnical characteristics of its shallow layers, the Valley of Mexico has been divided into three regions (top of Figure 1): (1) the hill zone with a surface layer of volcanic tuffs or lava flows, (2) the lake-bed zone consisting of 10 to more than 100 m of clays underlain by sands, and (3) the transition zone, consisting of alluvial sandy and silty layers, with occasional clay layers. The dramatic amplification of seismic waves in the lake-bed zone of the valley is a well-known and a reasonably well understood phenomena (Singh *et al.*, 1988 a,b). It is also the principal cause of damage suffered by Mexico City during large and great subduction zones and intraplate earthquakes. Recently, it has been shown that the thickness of the sediments is a parameter that influences the spectral accelerations during large earthquakes felt in Mexico City (Asimaki *et al.*, 2020).

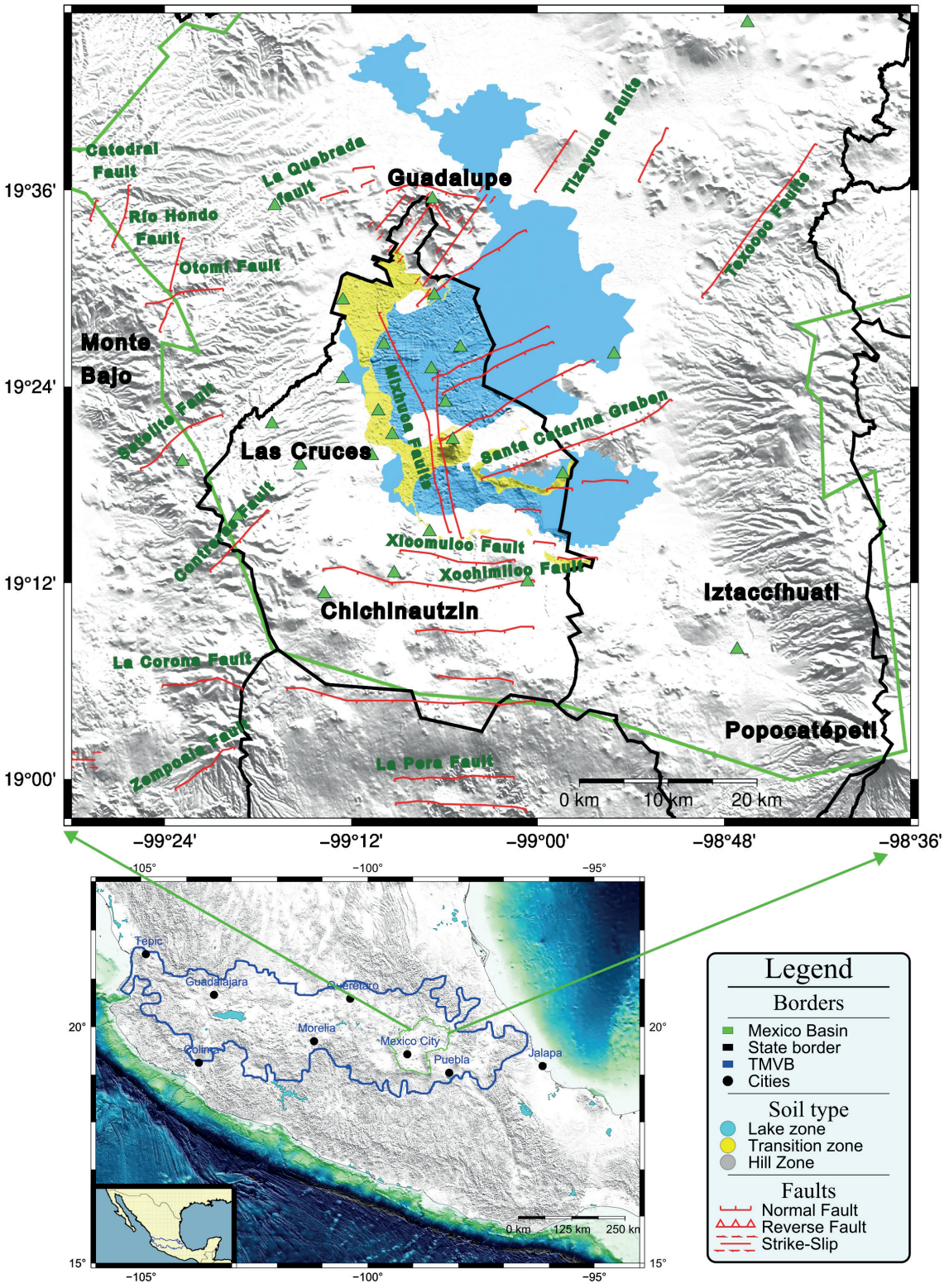

Figure 1. Top: image corresponds to the location of the Mexico basin in the central part of Mexico. Within the Basin of Mexico is located the Mexico City (black line). The names of the hills are highlighted in black lettering; green triangles are the stations of the Valley of Mexico seismic network Also, the names of the principal faults are highlighted in green lettering. (maps modified from Ferrari, *et al.*, 2012 and Arce, *et al.*, 2019). Bottom: Trans-Mexican Volcanic Belt (TMVB) (blue contour). Also shown by green contour is the Mexico Basin area.

3. Previous studies

Although the seismicity in the Valley of Mexico is of low magnitude, its study is crucial because of the high population density in this area of the country; in particular, the shallow activity (< 2 km) is likely to continue causing damages. On the other hand, the seismicity in the valley often has swarm-like characteristics as reported by Figueroa (1971) and Manzanilla (1986).

In the past, isolated efforts were made to characterize the failure type of different local events; unfortunately, because of the scarce seismic instrumentation available until a few years ago, it had only been possible to determine the fault type of some of these events. In one of the first studies, Havskov, (1982) analyzed an earthquake swarm which occurred west of Mexico City in February 1981; five of the largest events were analyzed obtaining a spectral seismic moment in the range of 0.5 - 2.0 x 10^{20} dyn-cm and rather low stress drops (1 – 5 bars). The first-motion distribution for the February 4 earthquake (M_L 3.1), allowed to determine a normal fault plane solution with an almost east-west oriented tensional axis. Table 1 displays the focal mechanism of this event.

Another study worth mentioning was that by UNAM and CENAPRED Seismology Group (1995). They analyzed an earthquake of M_c 3.9 which occurred on January 21, 1995 near the town of Milpa Alta. Using an algorithm on the basis of first-motion data, polarities of SV_z and SH phase, and P_z/SH and SV_z/SH ratios measured on displacement broadband seismograms, they calculated a focal mechanism associated to a normal-faulting event with significant (50%) strike-slip component, also shown in Table 1.

On October 16, 2005, an M_w 2.8 earthquake occurred in the urban area of Tlalpan, south of Mexico City. Quintanar, L., (unpublished data) calculated its seismic moment tensor with stations at local distances yielding a left-lateral strike-slip rupture with strike 118° from north, (Table 1).

Since 2010, the seismic network in the Mexico basin has been reinforced (Quintanar *et al.*, 2018) with the installation of more broadband sensors and accelerographs in several sites of Mexico City and some municipalities in the State of Mexico (see Figure 1). This expansion has enabled us to better pinpoint locations and record high-quality data. Importantly, it has opened up new avenues for a detailed study of small local earthquakes in the basin, such as the determination of focal mechanisms through moment tensor inversion (Singh *et al.*, 2020, Quintanar *et al.*, 2024). Next, we describe the techniques used to determine their faulting types.

4. Methodology

In the present study, we determine focal mechanisms for 24 local earthquakes from 2010 to 2024 with magnitudes greater than 2.5 recorded at least at three stations with clear P and S onsets (except Event 18, whose final inversion was performed with two stations). During this period, a sufficient number of stations recorded many earthquakes to yield reliable solutions. With these solutions, we obtain the stress field in different basin zones to understand the local tectonic characteristics. Three techniques have been applied to their analysis.

4.1 Moment Tensor Inversion (ISOLA)

MT inversion was performed using the ISOLA algorithm (Sokos and Zahradnik, 2008). This algorithm allows for both single and multiple point source iterative deconvolution inversion of complete regional and local waveforms using the method of Kikuchi and Kanamori, (1991). Moment tensors are obtained by a least-squares inversion, whereas a grid search over a range of candidate positions and time shifts is used to determine the location and origin time of point sources. A correlation coeffi-

Table 1. Previous work on focal mechanism solution of local earthquakes: (1) Focal mechanism obtained by Havskov, 1982 (westward zone). (2) Focal mechanism obtained by UNAM and CENAPRED Seismology Group, 1995 (southeast zone). (3) Focal mechanism calculated by L. Quintanar, (unpublished data) (south zone).

Event ID	Date yyyy-mm-dd	Origin Time UTC	Latitude	Longitude	Depth	Mag.	Strike	Dip	Rake	Beach Ball Image
1	1981-02-04	13:40:26	19.378	-99.196	1.2	3.1	320	10.1	-105	
2	1995-01-21	05:51:52	19.18	-98.97	12	3.9	106	63	-39	
3	2005-10-16	14:12:36	19.260	-99.267	10.3	2.8	118	74	-24	

cient is then calculated for each candidate to assess its fit with observed and synthetic waveforms.

While the 90% correlation threshold (i.e. $\geq 0.9 \times$ maximum correlation) is not mandatory for location or origin time determination, it is used later to identify and evaluate solutions. If no solution exceeds this threshold, the inversion may still yield a best-fit solution, but its reliability is low. Further assessments using indicators like signal-to-noise ratio (SNR), condition number (CN), or focal mechanism variability (FMVAR) are recommended.

This approach enables users to distinguish between well-constrained and potentially unreliable solutions, rather than rejecting all those below the 90% threshold. Green's functions, including near-field terms, are computed using the discrete wavenumber method (Bouchon, 1981; Bouchon and Coutant, 1994; Coutant, 1989).

ISOLA calculates several error parameters that are used to quantify the uncertainty in each solution. Each one of those parameters is not significant on its own, therefore, a joint interpretation of all the parameters must be made. The user is responsible for the correct interpretation of the results to avoid interpretations without physical meaning.

The signal-to-noise ratio (SNR) is a parameter that quantifies how much the signal of a seismic event reaches above the noise, calculated from the spectral amplitude of the signal. To do this, ISOLA program converts the signal in the time domain to the frequency domain applying a Fourier transform. Next, the ratio of the spectral amplitude of the signal to the noise is calculated. A high SNR value indicates that the event is easily recognized within the time window, while a low SNR value means that the amplitude of the event is comparable to the noise present in the waveform (Sokos and Zahradník, 2013).

A useful indicator for the quality of a solution of the Moment Tensor inversion can be obtained by quantifying the variability of the focal-mechanism solution near the best epicentral location and origin time. From all acceptable solutions with respect to the best-fit solution, specified by the user-defined correlation threshold, the Focal-Mechanism Variability Index (FMVAR), defined as the mean angle in space needed to rotate one set of axes into the other (Kagan, 1991), is calculated. A large value of the FMVAR indicates that the moment tensor inversion is unstable; conversely, when the focal mechanism solution is stable in the neighborhood of a source with maximum correlation, the FMVAR will be small (Sokos and Zahradník, 2013). Figure 2 shows a Flowchart with the description of inversion processus with ISOLA.

4.2 Source Inversion at short distances (INVERS2)

This method, hereafter named INVERS2, is described by Singh *et al.* (2000). It retrieves source parameters of small and moderate earthquakes recorded at short distances. The inversion assumes that such events may be approximated by a point source

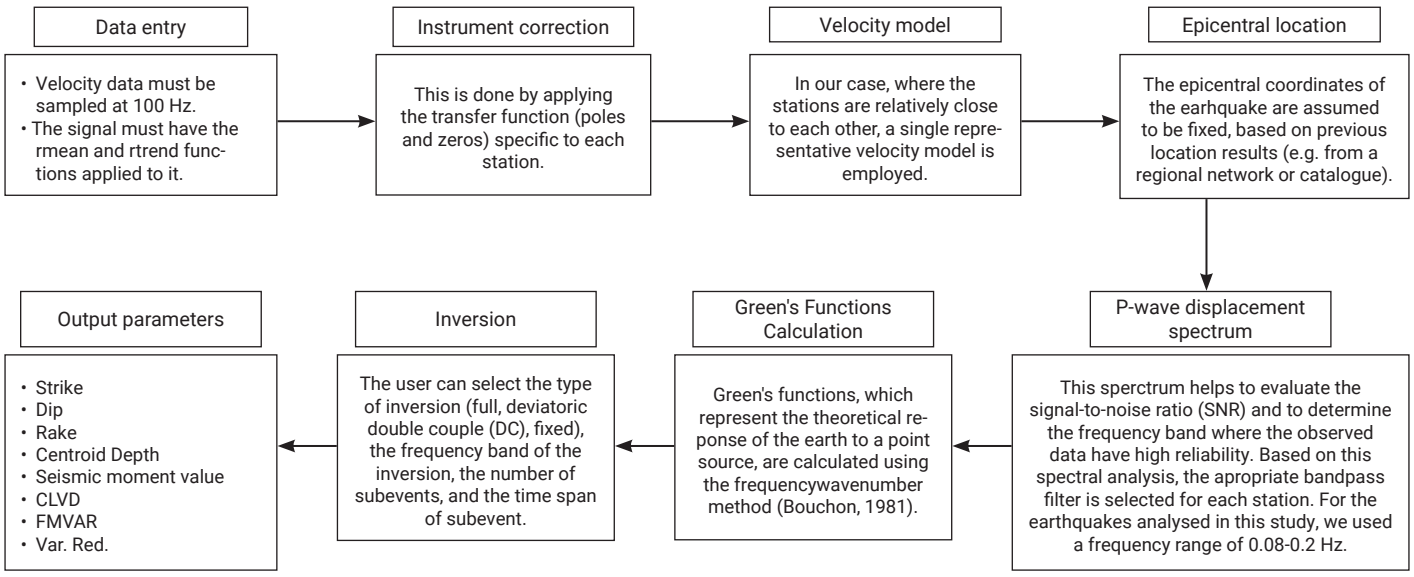

Figure 2. Illustrating the eight key steps with ISOLA seismic waveform inversion. It begins with high-resolution data sampling and instrument response correction. A fixed epicentral location is used, while source depth remains variable. The process continues with spectral analysis, Green's function computation, and inversion within a defined frequency range. Results are presented graphically, display moment tensor solutions, waveform fits, and misfit evaluations to assess inversion reliability.

shear dislocation, and the medium may be considered half-space. Synthetic seismograms used in the inversion include near- and intermediate-field contributions. The free surface effect is approximated by multiplying the synthetic seismograms computed in an infinite medium by a factor of two. This first-order correction emulates the amplification at the earth's surface without the need for more complex models and is equivalent to an approximate representation of a half-space medium. Although simplified, this approximation has proven to be effective in applications with near-source recordings, where near-field terms dominate the waveforms, and the location of the event is assumed to be known. A grid search is performed to determine the focal mechanism and the seismic moment that minimizes the misfit between the observed and the synthetic seismograms.

The observed seismic data are integrated to obtain displacement waveforms and adjusted by cutting and baselining to obtain records starting at P-onset and finishing after the arrival of the S-phase to identify the P and S-wave phases. Subsequently, the inversion process begins with assigning input parameters such as the seismic moment and the source time function shape, which is chosen on the basis of the P-waveform and may vary between triangular, trapezoidal, or other arbitrary forms.

Before inversion, it is essential to define a priori parameters such as hypocentral distance, azimuth, incidence, take-off angles, and a representative velocity model for the region. Synthetic seismograms are then generated and compared with the observed seismograms. From the solutions proposed by the inversion algorithm, one of the five with the lowest misfit is selected based on the regional tectonic context. Each solution provides the parameters of the fault plane (azimuth, dip, slip), the seismic moment, and the associated error, contributing to a more constrained and geologically consistent interpretation. Figure 3 shows a Flowchart of the inversion with INVERS2.

4.3 Stress field inversion

The inversion for the stress tensor in each zone was based on the Win-Tensor program (Delvaux and Barth, 2010; Delvaux and Sperner, 2003). The program assumes that stress is uniform in space, time-invariant and that earthquakes slip along the maximum shear stress direction. It is on the basis of: (1) a graphical method called Right Dihedron (Angelier and Mechler, 1977) and (2) an iterative Rotational Optimization method (Delvaux and Sperner, 2003) which minimizes the slip deviation between the observed slip line and the resolved shear stress favoring slip on the fault planes. We determined four parameters of the reduced tectonic stress axes σ1 (SHmax), σ2 (intermediate), σ3 (Shmin), where $\sigma1 \geq \sigma2 \geq \sigma3$ and the stress ratio $R = (\sigma2 - \sigma3)/(\sigma1 - \sigma3)$ and $0 < R < 1$ which expresses the magnitude of σ2 relative to the magnitudes of σ1 and σ3. This method also numerically expresses the stress regime index R′ numerically based on R and the most vertical stress (Delvaux and Barth, 2010), as follows:

$R' = R$	when σ1 is vertical (extensional stress regime)
$R' = 2 - R$	when σ2 is vertical (strike-slip stress regime)
$R' = 2 + R$	when σ3 is vertical (compressional stress regime)

The stress regime is expressed as normal-faulting (NF), strike-slip (SS), thrust-faulting (TF), intermediate between NF and SS (NS), intermediate between SS and TF (TS), and unknown or oblique (UF). Additionally, it provides the quality ranking parameter (Q) as defined by the World Stress Map (Heidbach *et al.*, 2010). The quality ranking (A, B, C, D) for fault slip has so far been defined considering the best fitting mean deviatoric stress tensor using Quaternary faults. This quality ranking also depends on the number of data and the

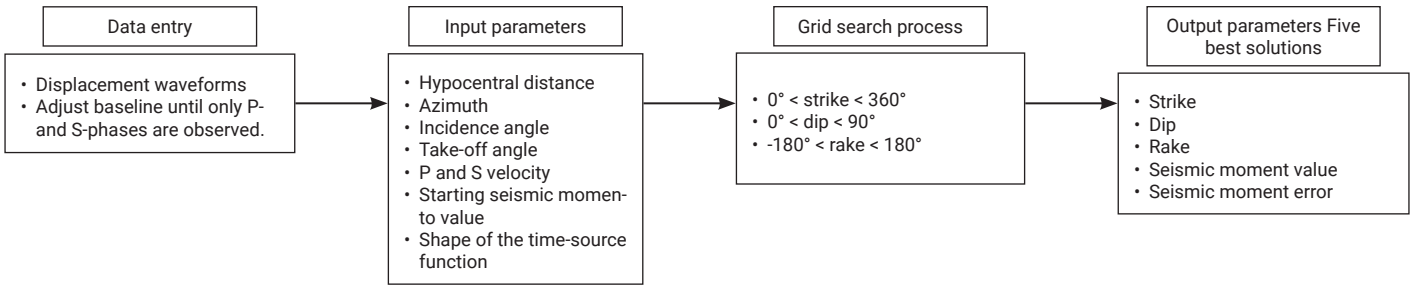

Figure 3. Flowchart showing the main steps for preparing seismic data for inversion using INVERS2. The process begins with data integration to obtain displacement waveforms and baseline correction to highlight P- and S-wave phases. Then, key input parameters are assigned, such as seismic moment and source time function shape. Finally, essential a priori information is required, including hypocentral distance, azimuth, incidence and take-off angles, and the local velocity model.

average misfit between calculated and theoretical slip direction. The 1σ standard deviations for the compressive stress regime (σ1), the extensive stress regime (σ3) (SHmax/Shmin), and R′ are determined by the uncertainties associated with σ1, σ2, σ3, and R.

5. Data and processing

We grouped the selected 24 events according to their epicentral location into five families, which we will call: (a) Sierra de las Cruces (SC), (b) Central zone (C), (c) Southeastern zone (SE), (d) Lake-bed zone (LB), and (e) Sierra Chichinautzin (CH).

5.1 Velocity models

Three velocity models were used depending on the location of the earthquakes: for the seismicity west of the city, we used the crustal model proposed by Singh et al, (2020), which has been modified from Havskov (1982). This model is shown in Table 2; the P-wave velocity α, of the top two layers, is based on a refraction study by Havskov and Singh (1978).

The second model is for the Southeastern zone (Table 3). The difference to the model for the western earthquakes lies in the attenuation parameters and the velocities of the first two layers. The velocities of the upper 5 km are on the basis of the refraction study conducted by Havskov and Singh (1978), on a few bore-hole measurements (Marsal and Graue, 1969; PEMEX, 1986), and seismic reflection profiling (Flores López, 1987; Perez Cruz, 1988). Below 5 km the structure is on the basis of a surface wave dispersion study by Campillo *et al.* (1996).

For the rest of the analyzed seismicity, we used a velocity model modified from Havskov and Singh (1978), and calculated from unreversed seismic refraction profiles, using quarry blasts as source and adjusting theoretical and observed arrival times, shown in Table 4. In general, the earthquakes' depth was deter-

Table 2. Velocity model for Sierra de las Cruces (Singh *et al.*, 2020)

Thickness [km]	α [km/s]	β [km/s]	ρ[gr/cm^3]	Q_α	Q_β
2	2.9	1.58	2.5	100	50
2	4.7	2.72	2.76	100	50
26	6.6	3.81	2.82	100	50
5	7.1	4.1	3.03	100	50
400	8.1	4.68	3.14	100	50

Table 3. Velocity model for the Southeastern area (UNAM and CENAPRED Seismology group, 1995)

Thickness	α [km/s]	β [km/s]	ρ[gr/cm^3]	Qα	Qβ
2	2.9	1.6	2.28	200	100
2.3	4.9	2.85	2.68	200	100
4.7	5.82	3.38	2.86	400	200
36	6.55	3.81	3.03	400	200
400	8.1	4.7	3.32	800	400

Table 4. Empirical velocity model obtained from quarry explosion tests in the southern part of Mexico City (modified from Havskov and Singh, 1978)

Depth [Km]	Velocity α	Velocity β
	[Km/s]	[km/s]
0	2.9	1.7
2	4.7	2.7
5	6	3.5
12	6.8	3.9
23	7.7	4.5
45	8.1	4.7
100	8.3	4.8

mined using the subroutine RMSDEP in the SEISAN software, which calculates and plots RMS as a function of depth for the current event (Havskov *et al.*, 2020).

We extracted the events from the National Seismological Service database for the period 2010-2024, events with a magnitude greater than 2.5, good azimuthal coverage and events with a signal-to-noise ratio SNR > 20 were selected. Before the analysis of focal mechanisms, we relocated the 24 selected events; Table 5 displays the final location obtained as well as the velocity model used for each event. The M_w value shown is the result of the inversion process.

Due to the scarcity of available records for some events, where the nearest station is more than 8 km away and in general there is no good coverage of stations, we applied INVERS2 to invert six events with a magnitude greater than 2.5. Figure 4 provides an example of the results obtained with this technique and **supplemental material** shows the final results for the six events.

For events where the signal-to-noise ratio was SNR≥20, recorded at least in three stations, the focal mechanisms could be calculated using the ISOLA program. Although the focal mechanism was successfully computed using ISOLA software with data from only two stations for Event 18, the limited azimuthal coverage introduces significant limitations. Poor azimuthal distributions can lead to unstable or non-unique solutions, as the inversion is underconstrained in directions with little or no data coverage. This configuration increases the condition number (CN) of the Green's function matrix and often results in higher variability indices such as FMVAR and STVAR, indicating

Table 5. Earthquakes located in the Mexico basin and analyzed in this study. M_w was calculated with the inversion of the two techniques used. The hypocentral location was calculated using the software Seisan (Havskov *et al.*, 2020). Three different velocity models were used: Southeastern model (SE) (UNAM and CENAPRED Seismology Group, 1995); Sierra de las Cruces model (SC) (Singh *et al.*, 2020); Generic model (GM) (Modified from Havskov and Singh, 1978).

Event ID	Date yyyy-mm-dd	Origin Time UTC	Latitude	Longitude	Depth	Mw	Velocity model
1	2010-07-05	17:20:42	19.230	-98.920	11.9	3.0	SE
2	2012-07-09	00:29:19	19.300	-98.948	14.3	2.0	SE
3	2013-01-19	04:47:43	19.331	-99.158	4.5	3.0	GM
4	2014-07-19	11:57:21	19.150	-98.952	12.0	3.2	GM
5	2014-12-01	08:50:06	19.363	-99.227	0.8	2.6	GM
6	2015-04-06	20:53:05	19.175	-98.934	5.4	2.7	SE
7	2015-04-09	08:38:16	19.402	-99.072	0.4	2.4	SC
8	2017-03-01	09:56:52	19.338	-99.146	5.6	2.7	GM
9	2017-09-10	02:54:12	19.300	-99.181	7.6	2.9	GM
10	2017-10-28	06:52:36	19.222	-99.224	2.0	2.9	GM
11	2017-12-29	07:38:57	19.385	-99.164	1.0	2.0	SC
12	2018-02-13	21:39:38	19.460	-99.072	4.0	3.0	GM
13	2019-03-29	08:31:56	19.409	-99.218	1.0	2.3	SC
14	2019-07-17	03:53:00	19.409	-99.209	0.8	3.2	SC
15	2019-09-23	08:03:08	19.172	-98.946	10.8	2.6	SE
16	2020-06-07	14:45:21	19.374	-99.202	1.0	2.6	SC
17	2021-07-06	07:00:09	19.463	-98.970	5.4	1.6	GM
18	2022-05-23	11:58:28	19.480	-99.063	12.3	2.5	SC
19	2023-01-19	09:00:51	19.055	-99.110	10.7	3.0	GM
20	2023-05-11	04:20:19	19.364	-99.197	0.8	3.1	SC
21	2023-06-03	01:12:04	19.360	-99.180	1.0	1.3	SC
22	2023-12-12	17:07:53	19.363	-99.200	3.0	3.0	SC
23	2023-12-14	20:13:14	19.363	-99.200	0.3	3.2	SC
24	2024-02-14	12:42:13	19.374	-99.201	1.4	3.1	SC

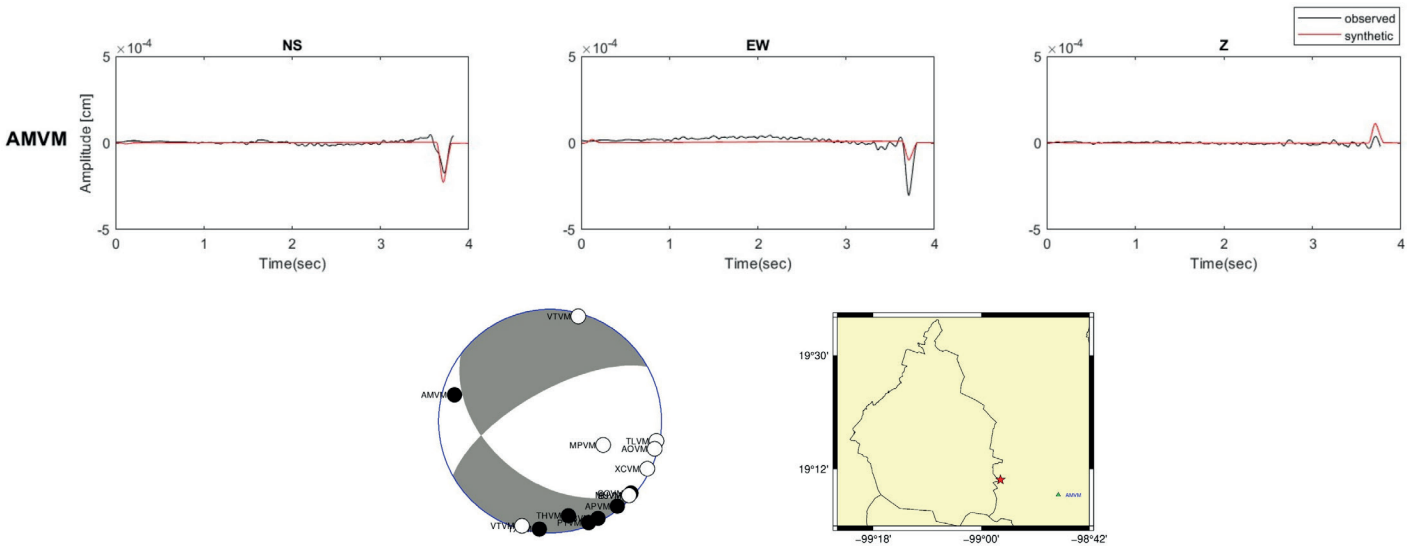

Figure 4. Example of solution obtained with INVERS2 in the Southeastern zone with an event which occurred on 2019/09/23 08:03:08 (UTC). Black and red traces are observed and synthetic displacement sesimograms. Beach ball shows the inverted focal mechanism and includes P-wave polarity read on the recordings. The map on the lower right gives the location of the event and the station used for the inversion.

reduced reliability and resolution of both the source mechanism and hypocentral parameters. In such cases, additional constraints such as first-motion polarities or tectonic context become essential to validate the solution and assess its physical plausibility

Figure 5 shows an example from each of the five regions. The Figure compares the observed and synthetic signals with the calculated focal mechanism below the graphs, including polarity readings. On the right side, the Figure shows the event and the station locations. This method was applied to 18 events, and the results are given in the **supplemental material**.

6. Results

6.1 Distribution of focal mechanisms in the Mexico basin

The results of our analysis show that the faulting types within the Mexico Basin are not uniform between the different groups of events, which reflects a complexity in the geological structures of the region. Table 6 shows the focal mechanism solutions obtained for all the events studied. Although there is a preponderance of normal faults and strike-slip faults, we observe a great diversity in the strike value of these faults.

Figure 6 displays the location and focal mechanism solutions obtained for the studied earthquakes. We emphasize that separation by groups of events is on the basis of the distribution of seismicity within the Valley of Mexico in five zones a) Sierra de Las Cruces, b) Central area, c) Southeastern area, d) Lake-bed area in the Mexico basin and e) Chichinauitzin area.

6.2 Stress field inversion

We performed a local stress field analysis with these focal mechanism solutions to detect variations that allow us to infer how these stresses affect the activation of previously mapped faults. The corresponding parameters obtained are listed in Table 7, and a detailed analysis of them is discussed in Section 7. It's worth noting that during the period analyzed (2010-2024), 15 events were located within the Sierra de Chichinautzin area, of which only two were susceptible to inversion (SNR > 20) at the nearest stations (events 10 and 19). The distance between these earthquakes is 16 km, posing a significant challenge in associating them with the same geomorphological area and, therefore, determining the stress field. According to Table 6, we can just affirm that the stress axes of these events are oriented in an NW-SE direction. This lack of enough well-recorded earthquakes highlights the scarcity of seismic stations south of Mexico City, an important issue because this zone is located in the volcanic field closest to Mexico's main urban area.

Figure 7 shows the stress field in the four zones a) Sierra de Las Cruces, b) Central area, c) Southeastern area and d) Lake-bed area in the Mexico basin. The results are represented by the function of the stress regimes and horizontal stress axis orientation. Although the dominant tectonic regime is extensional (NF) in most of the basin, in the central area, the dominant mechanism is strike-slip (SS).

The results of the stress field inversion show that the dominant tectonic regime is extensional and transtensional. At Sierra de las Cruces, normal-faulting (NF) is the dominant tectonic

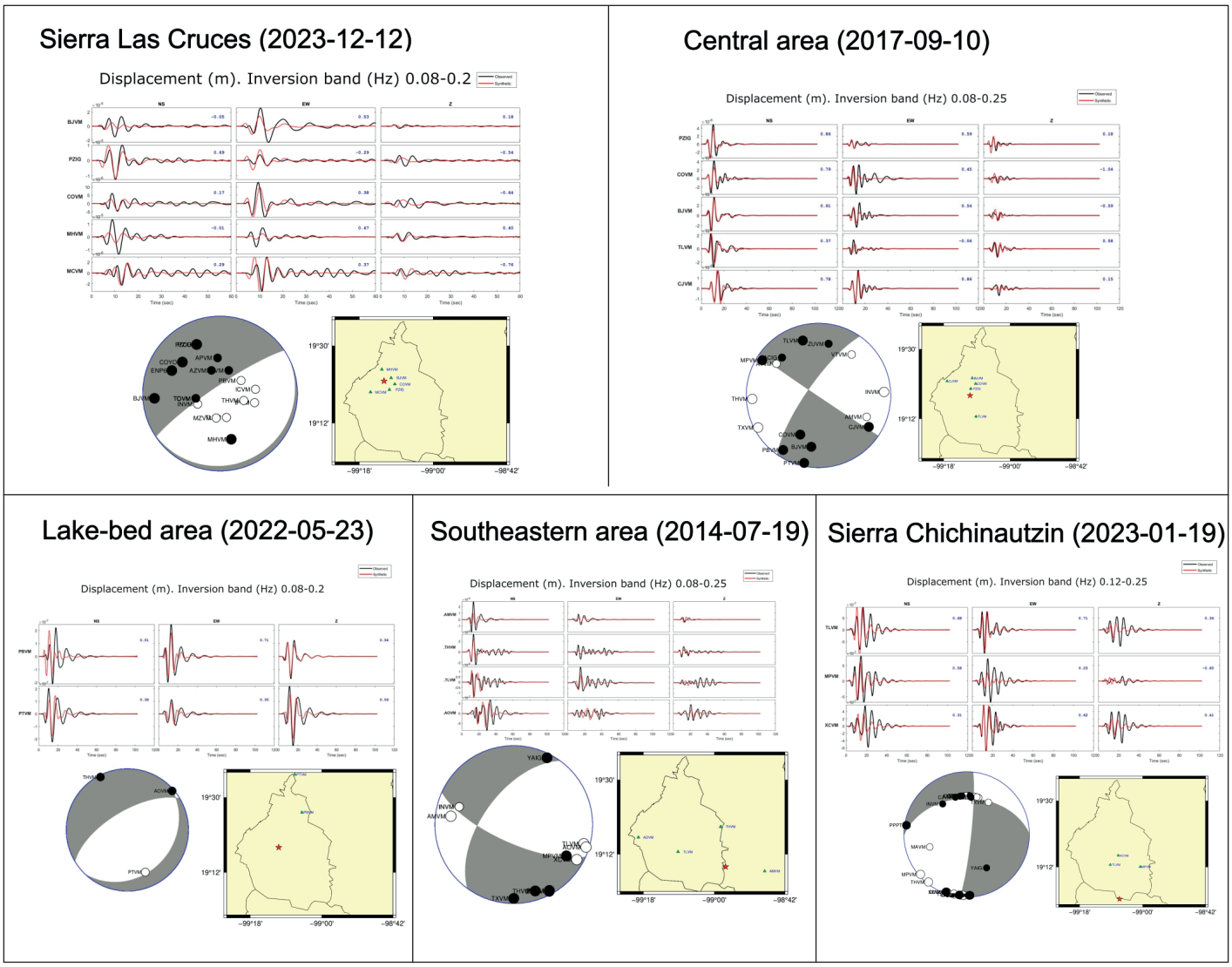

Figure 5. Examples of the waveform modeling with ISOLA. Black and red traces are observed and synthetic, filtered displacement sesimograms. Beach ball shows the inverted focal mechanism and includes P-wave polarity read on the recordings. The map on the lower right gives location of the event and the stations.

regime, trending approximately NW-SE, whereas the dominant tectonic regime in the central area is strike-slip (SS). In the Southeastern and the lake-bed regions, the stress field inversion reveals normal-faulting with an extensive stress regime in the NE–SW direction.

We are observing a mixed stress field, which means that there are faults not yet subject to geophysical or geological studies. Following the obliquity of the TMVB it is not rare to find this type of mixed faulting mechanisms in this region, which shows that the stress field in the basin is not completely extensional. Near the Sierra del Chichinautzin, its behavior is strike-slip, as can be observed in the earthquakes of the central, southern and southeastern regions.

Moreover, using well-defined focal mechanisms, new poles of rotation, and accurate bathymetry, Ego and Ansan (2002) concluded that the active zone of the east-west (E-W) striking Trans-Mexican Volcanic Belt (TMVB) in central Mexico is dominated by active normal faults with a left-lateral strike-slip component striking E-W. Their study shows that the stress state in the central TMVB has been transtensional since the Middle Quaternary, with Shmin (σ3) oriented NW-SE and Shmax (σ1 or σ2) oriented NE-SW. Oblique convergence and slip partitioning at the trench induce this stress state, the central TMVB is not parallel to the trench as the geometry of the subducted plate influences the orientation of the volcanic arc, causing a 20° deviation in counterclockwise direction. Our results show the coexistence of extensional and lateral slip tectonic stress fields because of the existence of a region of oblique extension. From Table 7, it can be seen that in this region the principal intermediate stress σ2=81° is close to vertical, generating horizontal

Table 6. Results of the analysis of the earthquakes corresponding to the Event ID in table 5.

Event ID	Inversion Technique	Centroid depth ISOLA	Frequency band	Plane 1	Plane 2	P	T	FMVAR	Var-red	Beach Ball Image
				Strike/Dip/ Rake	Strike/Dip/ Rake	Azimuth/ Plunge	Azimuth/ Plunge			
1	Invers2	10		21/34/-180	291/90/-56	230/36	352/36			
2	Invers2	--		318/45/-42	81/61/-126	301/57	196/9			
3	Isola	4	0.08-0.2	358/86/171	88/81/4	43/4	313/9	7±11	0.38	
4	Isola	11.1	0.1-0.3	97/33/127	35/64/69	341/17	109/64	16±8	0.39	
5	Isola	0.5	0.08-0.2	99/30/131	234/68/69	340/20	111/61	16±8	0.39	
6	Invers2	--		64/45/-148	310/68/-50	265/50	12/14			
7	Isola	0.6	0.3-0.5	147/41/37	27/67/125	93/15	341/54	25±24	0.63	
8	Isola	3.6	0.08-0.2	285/87/-31	17/59/-176	236/24	335/19	22±14	0.27	
9	Isola	4.5	0.08-0.2	215/77/-179	124/89/-13	79/10	170/8	28±33	0.64	
10	Isola	8.5	0.08-0.2	202/79/-121	94/33/-21	80/47	316/27	43±38	0.23	
11	Isola	0.8	0.15-0.27	191/76/-158	94/69/-18	53/27	322/3	37±23	0.69	
12	Isola	4.9	0.1-0.23	271/11/-76	77/79/-93	343/56	169/34	11±6	0.40	
13	Isola	1	0.1-0.22	281/31/-102	114/60/-83	49/74	205/15	18±11	0.69	
14	Isola	1	0.08-0.2	228/80/-97	82/12/-57	129/54	324/35	17±21	0.70	
15	Invers2	--		254/56/-127	128/48/-48	106/60	9/4			
16	Isola	1.2	0.16-0.28	235/82/-112	127/23/-20	122/48	344/33	19±18	0.42	
17	Invers2	5		233/90/106	323/16/0	308/43	158/43			
18	Isola	8.2	0.08-0.2	239/65/-84	44/25/-104	161/69	324/20	9±6	0.47	
19	Isola	11.7	0.12-0.25	6/84/-132	269/42/-9	240/37	128/27	21±14	0.45	
20	Isola	0.7	0.08-0.24	270/76/-75	42/20/-136	199/56	348/29	27±24	0.53	
21	Invers2	--		244/68/-180	334/90/22	107/15	201/15			
22	Isola	0.5	0.08-0.2	63/8/-83	236/82/-91	145/53	327/37	13±11	0.34	
23	Isola	0.6	0.08-0.2	259/89/-86	4/3/-165	173/46	345/44	15±11	0.58	
24	Isola	0.7	0.08-0.24	221/83/-109	111/20/-21	111/49	327/35	21±15	0.71	

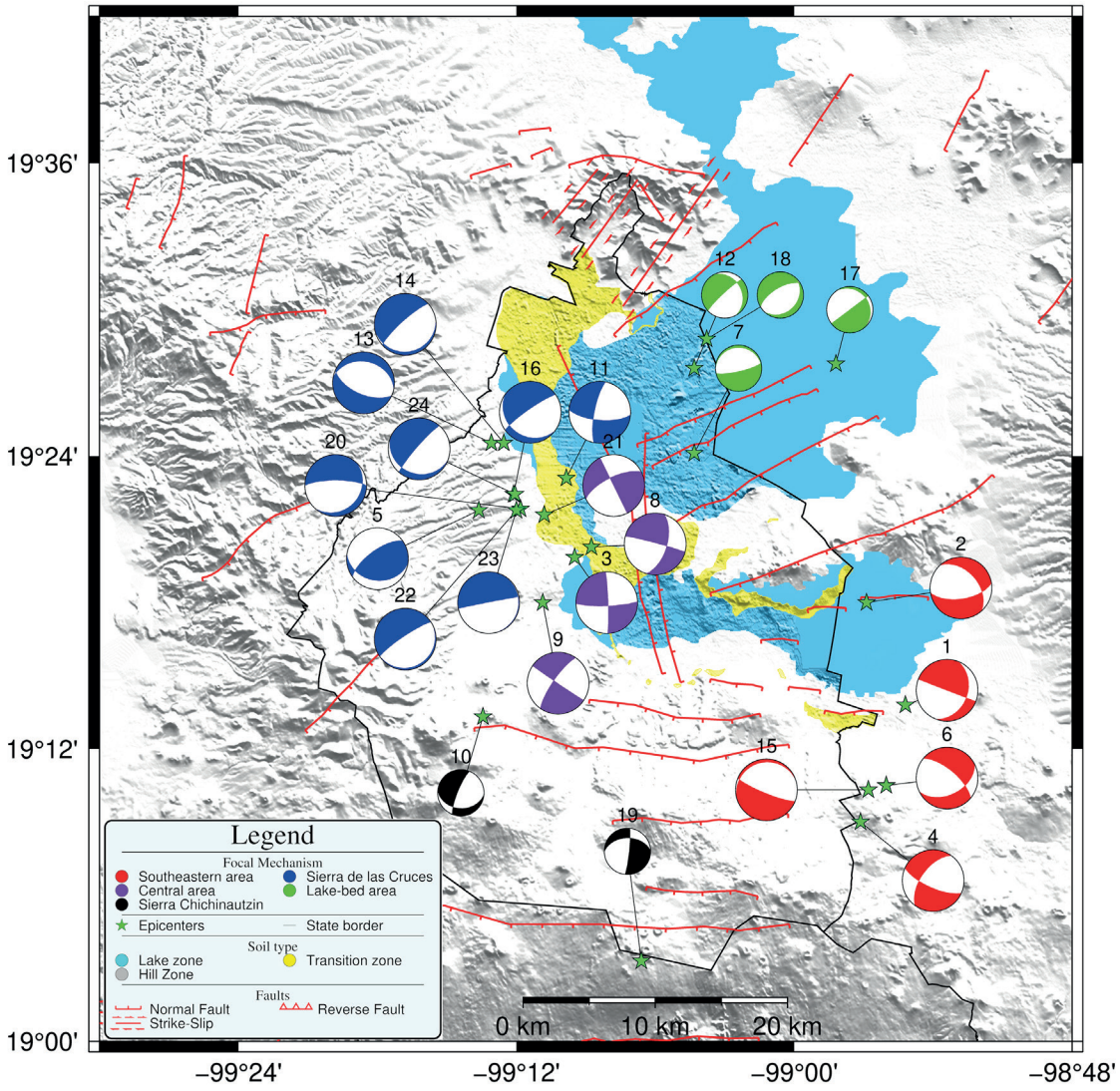

Figure 6. Results of the analysis of 24 events. focal mechanisms are classified by their location. Colors of beach-balls represent the families of events in five zones a) Sierra de Las Cruces, b) Central area, c) Southeastern area, d) Lake-bed area in the Mexico basin and e) Chichinauitzin area.

Table 7. Stress field inversion for each zone. Stress tensor parameters according the World Stress Map: σ1, σ2 and σ2: principal stress axes; azimuth; plunge; a, average misfit angle; Q: quality; A or B mean very good quality whereas C indicate medium quality; Reg: stress regime (NF: normal faulting; SS: strike–slip faulting) ; R′: numerical stress regime; Shmax and Shmin: maximum (σ1) and minimum (σ3).

Area	Number of focal mechanism solutions	Reduced stress tensor parameters						Quality		Tectonic Stress Regime			
		σ1 plunge	σ1 azimuth	σ2 plunge	σ2 azimuth	σ3 plunge	σ3 azimuth	α Ave.	Q	Reg.	R′	Shmax	Shmin
a) Sierra de la Cruces	7	50	139	6	236	39	331	23.1	B	NF	0.88	67	157
b) Central	3	30	63	81	172	9	333	17.5	C	SS	1.5	69	159
c) Southeastern	5	78	172	2	261	12	351	27.9	C	NF	0.5	81	171
d) Lake-bed	3	60	54	25	197	16	294	56.5	C	NF	0.5	32	122

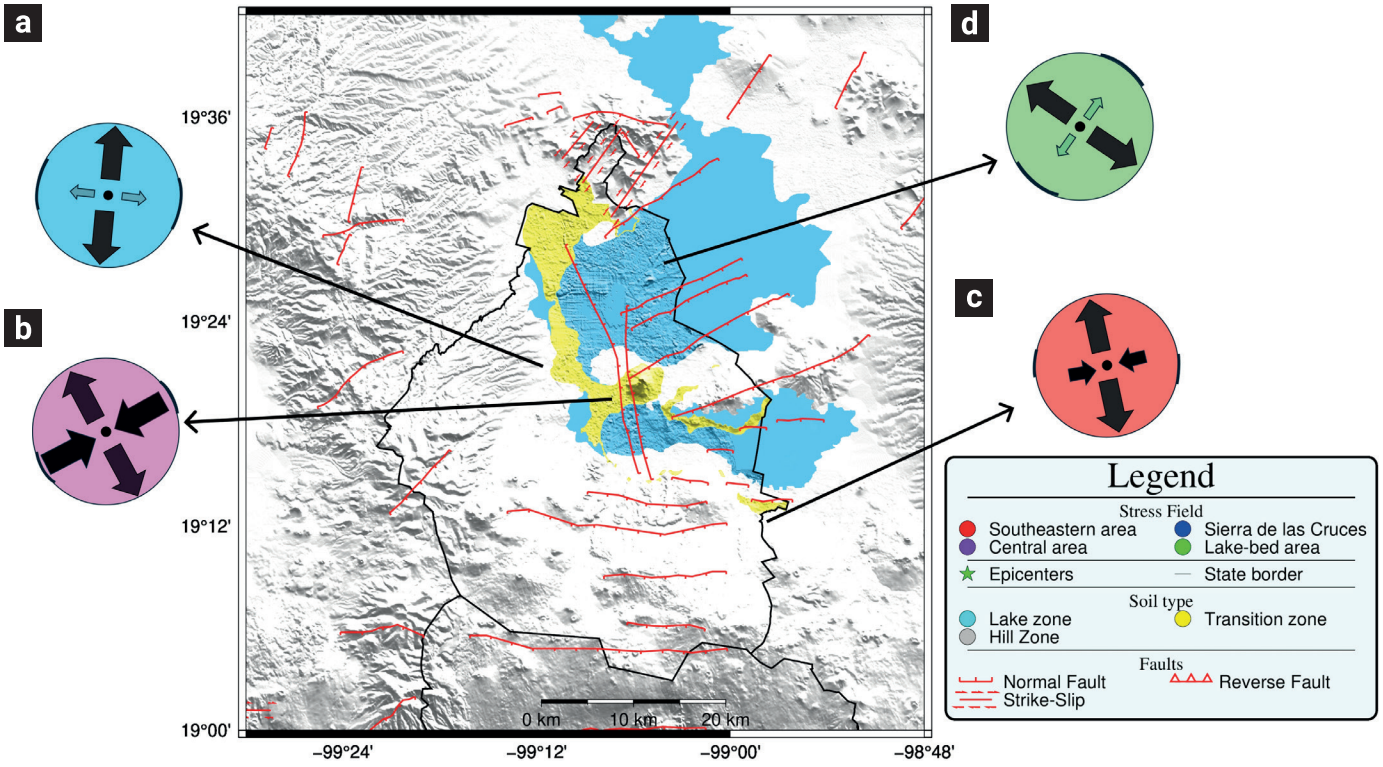

Figure 7. The map shows the stress field in every area, and the corresponding faults and soil type obtained with Win-Tensor package (Delvaux and Sperner, 2003; Delvaux and Barth, 2010). Results obtained for every area in Mexico basin a) Las Cruces Hills, b) Central area, c) Southeastern area and d) Lake-bed areas in Mexico basin.

shear deformation, compared to the value of σ1=50° in Sierra de las Cruces, σ1=60° the lakebed and the σ1=78° southeastern region, which have a vertical σ1 principal axis and generate extensional deformation.

7. Discussion

7.1 Sierra de las Cruces

This area, located in the central part of the Sierra de las Cruces, is where the shallowest earthquakes are recorded and, therefore, are the most strongly felt by the population. According to García-Palomo *et al.* (2008), the presence of the Lomas Trench (Mooser *et al.*, 1992), a structure delimited by the Satellite fault and the Contreras fault, with a general trend of N53ºE, is one of the causes of the regional subsidence of the central block of the Sierra de las Cruces.

Among the well-studied events in this zone of the Valley of Mexico is a swarm-like activity near the Tacubaya (TAC) seismological station in 1981 (Havskov, 1982). On the other hand, the swarm-like activity that happened in the city in June-August 2019 was well recorded in 44 sensors. This sequence also occurred close to TAC, about 4 km north of the 1981 sequence. The most significant event of the 2019 sequence, an M_w 3.2 earthquake on 17 July, caused great panic in some of the neighborhoods of the city and generated peak ground acceleration (PGA) exceeding 0.3 g at the closest station about 1 km away (Singh *et al.*, 2020). Analysis of the large dataset produced by the sequence presented unusual difficulties owing to the complex upper crustal structure and highly variable superficial layers of the Valley of Mexico.

On 11 May 2023, a local earthquake in the city was strongly felt in Mixcoac, San Angel, and Coyocán. The quake was preceded and followed by events that were also alarming to the population. The events in the 2023 sequence were located about 5 km south of the 2019 sequence, with most events occurring within 2 km of the 1981 sequence. The 11 May 2023 earthquake produced a PGA triplet of (152, 139, 178 cm/s^2) on the NS, EW, and Z components (Quintanar *et al.*, 2024). Based on our stress field analysis in this area, the dominant tectonic regime is extensional (NF) trending approximately NE-SW; this direction is the same of strike of faults system reported by García-Palomo *et al.* (2008). Havskov (1982) suggested that the sinking of the Valley of Mexico could possibly produce similar

oriented tensions as those accumulated in this zone, which, if not causing the earthquakes, might trigger them. In a recent research, Aguilar-Velázquez *et al.* (2025) propose that this swarm activity is the result of interaction of two mechanically distinct zones: a stable region prone to aseismic deformation to the east where faults are buried under water-saturated sediments, and an unstable region to the west, prone to seismic radiation where faults are expressed geomorphologically.

7.2 Central area

According to reports from the Seismological Service of Mexico, in this area, there are 62 events, all of them with magnitudes less than 3.2; the largest event occurred on 2010-06-24 at 15:36:17 (UTC) and was located 3 km southeast of Benito Juárez in Mexico City. However, there are only four earthquakes suited for analysis because most of them have magnitudes of less than 2, contrary to seismicity to the west of Mexico City. A fact worth noting is that there are not enough broadband sensors near the epicenter, and for the analysis of those small magnitude events it is, therefore, essential to increase the number of broadband sensors in this area. On the other hand, as shown in Figure 6, the focal mechanism solutions indicate strike-slip faulting, and the stress field in Figure 7 shows a right-lateral strike-slip regime, which agrees with the regional tectonic setting (Arce *et al.*, 2019).

The coexistence of two tectonic stress fields, one extensional and the other strike-slip, could be because of the interaction of different tectonic forces producing a mixed stress regime. In this case, the tectonic forces in the TMVB driving extension are not perfectly perpendicular to the main boundary or structure, and an additional shear component is generated. For example, in rifts such as the East African Rift, oblique extension leads to the coexistence of normal and strike-slip faults (Delvaux and Barth, 2010).

7.3 Southeastern area

Some events of this area have been analyzed in the past (UNAM and CENAPRED Seismology Group, 1995). According to the results in Figure 6 we observed mechanisms with mostly normal-faulting with one of the planes having an approximately E-W strike and only one with a significant strike-slip component. It is essential to highlight that, according to Arce *et al.* (2019), this area is characterized by the presence of normal faults trending E-W, primarily associated with the Sierra de Chichinautzin on the southern limit of the Basin of Mexico (see Main Map therein). The stress field in this area indicates an extensional regime in the N-S direction. The average depth of this activity is around 15 km. Campos-Enríquez *et al.* (2015) studied the tectonics and seismicity of this zone. Using composite focal mechanisms to characterize the source parameters of seismic activity, they determined two nodal planes: one of them dipping north (and corresponding to a normal fault) would correlate with the normal Xochimilco Fault. The second solution describes a NW-SE right-lateral transcurrent mechanism, where no fault has been mapped.

7.4 Lake-bed area

This area, situated at the former lake of Mexico City, is known for its unique seismic activity. While low-magnitude earthquakes have been recorded, what sets these apart from other regions is their significant depth, often exceeding 5 km. This is a region with a high population density and crucial facilities such as the Mexico City International Airport, which could be significantly impacted by earthquakes. Despite seismicity not being very frequent, seven earthquakes have occurred. The stress field inversion analysis reveals that normal faulting has an extensional stress regime oriented in NW-SE direction. This regime aligns with a series of normal and dextral strike-slip faults, both with NE-SW trend, which might be related to the Tenochtitlan mega shear zone (De Cserna *et al.*, 1987; García-Palomo *et al.*, 2008).

7.5 Sierra Chichinautzin

Our analysis at Sierra Chichinautzin has shed light on two earthquakes, as depicted in Figure 6. These earthquakes exhibit a strike-slip focal mechanism with right-lateral displacement. This finding is particularly significant when compared to the Campos-Enríquez *et al.* (2015) study of the Aztlán fault system, which reported an NW-SE to N-S extension with minor E-W left-lateral movement. Additionally, the moment tensor inversion by Quintanar, L. (unpublished data) for the earthquake on October 16, 2005 (Table 1), using MASE stations (Pérez-Campos *et al.*, 2008), also hints at a strike-slip fault oriented in NW-SE direction. It is worth noting that no left-lateral faults are mapped in that direction. However, Márquez *et al.* (1999) reported that satellite images and volcanic alignment indicate a predominant E–W tectonic trend, with subordinate NNE–SSW, NNW–SSE, and NE–SW directions. These combined studies suggest the presence of unmapped strike-slip faults oriented NW-SE, like the Xochimilco fault.

8. Conclusions and future work

Despite its low magnitude, seismicity in the Valley of Mexico is of great importance because it occurs at shallow depths and in

the country's most densely populated area. Many authors have reported that earthquakes in different areas of the capital have caused fractures and cracks in low-rise buildings in the past. In this work, we have used the records of the Seismic Network of the Valley of Mexico, whose installation started in 2000 with a few stations but consolidated since 2010 with broadband seismometers and force-balanced accelerometers (Quintanar *et al.*, 2018) to obtain focal parameters for the first time systematically of the largest earthquakes ($M > 2.5$) whose frequency content has allowed the moment tensor inversion to be carried out.

Using the ISOLA software for multi-station waveform modeling inversion and the INVERS2 method for single-station inversion, moment tensors were obtained for 24 earthquakes located in the Valley of Mexico. In most cases, we found an agreement between the strike and type of faults reported at the epicentral zone, and the results of the focal mechanism solutions obtained.

We highlight the western area of Mexico City, where earthquakes have been felt with great intensity in the epicentral zone recently, causing panic among the population and concern among the authorities (Quintanar *et al.*, 2024). This seismicity has developed mainly in the central block of the Sierra de las Cruces fault system, where García-Palomo *et al.* (2008) reported regional subsidence of this geological feature. We also emphasize strike-slip faulting earthquakes in the central part of Mexico City that do not correspond to any identified fault. This underscores the need for further research and vigilance of seismic monitoring.

In general terms, our results show that active faulting in the Basin of Mexico is complex, even the faults already known and reported in previous studies are not necessarily associated with the earthquakes presented in this work. They probably occur on other faults near the known faults, which do not necessarily have to be extensional. We identified five areas where seismicity is concentrated: Sierra de las Cruces, Central area, Southeastern area, Lake-bed area, and Sierra Chichinautzin. These five regions are correlated with local tectonic faults or by soil type. Although the Sierra Chichinautzin zone could not be fully analyzed because of a lack of data and seismic activity, the focal mechanism analysis reveals the existence of strike-slip faults. A deeper search and monitoring of unreported failures is a subject that must be addressed from a multidisciplinary approach for our understanding of seismicity.

Finally, it is important to note that the stresses governing seismicity in the Basin of Mexico are highly specific to each zone. For example, the Sierra de las Cruces (westward to Mexico City) experiences a low magnitude shallow seismic activity that can cause significant peak ground accelerations and damage to older structures. Geotechnical features, such as the transition from hill to lake-bed zone, can create a complex network of tensional stresses because of differential subsidence. Anthropogenic phenomena, like water extraction, need to be rigorously assessed from a physical point of view (pore pressure changes, water flow variations, etc.) to evaluate their contribution to increasing tensional stress.

On the other hand, the Southeastern zone is of particular interest as it delineates the border of the Mexico basin with the Chichinautzin volcanic field. The earthquakes that occur in this region, while not always felt because of their depth, are most significant because of their magnitudes.

The complexity of the stress field in Mexico City could manifest the transtensional stress state in the central TMVB because of the oblique direction of the TMVB relative to the Middle America Trench.

9. Data and Resources

Data used in this study were obtained by the National Seismological Service (SSN; **https://doi.org/10.21766/SSNMX/SN/MX**), Instituto de Geofísica, UNAM.

10. Acknowledgments

The authors acknowledge incisive and helpful comments by two anonymous reviewers. We also thank the personnel of the Analysis Group at the National Seismological Service (SSN), Instituto de Geofísica, Universidad Nacional Autónoma de México (UNAM), as well as Arturo Cárdenas, who belongs to the Instrumentation Group, for their assistance with seismic network maintenance. The authors deeply acknowledge the support received from government authorities of Mexico City through their Secretaría de Educación, Ciencia, Tecnología e Innovación for acquisition of seismological equipments and its deployment through Funding Agreement SECTEI/045/2024. The research was partly supported by Dirección General Asuntos del Personal Académico (DGAPA), UNAM Project IN116423.

11. References

Aguilar-Velázquez Manuel J, Paulina Miranda-García, Víctor M. Cruz-Atienza, Darío Solano Rojas, Josué Tago, Luis A. Domínguez, Carlos Villafuerte, Víctor H. Espíndola, Delia Bello-Segura, Luis Quintanar-Robles, and Mathieu Perton, (2025); Interplay of slow-slip faults beneath Mexico City induces intense seismicity over months; *Tectonophysics*, 902, 230659. doi: **https://doi.org/10.1016/j.tecto.2025.230659**

Angelier, J., and Mechler, P. (1977). Sur une methode graphique de recherche des contraintes principales egalement utilisables en tectonique et en seismologie: la methode des diedres droits. *Bulletin de La*

Société Géologique de France, S7-XIX(6), 1309–1318. doi: **https://doi.org/10.2113/gssgfbull.S7-XIX.6.1309**

Arce, J. L., Layer, P. W., Macías, J. L., Morales-Casique, E., García-Palomo, A., Jiménez-Domínguez, F. J., Benowitz, J., and Vásquez-Serrano, A. (2019). Geology and stratigraphy of the Mexico Basin (Mexico City), central Trans-Mexican Volcanic Belt. *Journal of Maps*, 15(2), 320–332. doi: **https://doi.org/10.1080/17445647.2019.1593251**

Asimaki, D., Mohammadi, K., Ayoubi, P., Mayoral, J. M., and Montalva, G. (2020). Investigating the spatial variability of ground motions during the 2017 Mw 7.1 Puebla-Mexico City earthquake via idealized simulations of basin effects. *Soil Dynamics and Earthquake Engineering*, 132, 106073. doi: **https://doi.org/10.1016/j.soildyn.2020.106073**

Bouchon, M. (1981). A simple method to calculate Green's functions for elastic layered media. *Bulletin of the Seismological Society of America*, 71(4), 959–971. doi: **https://doi.org/10.1785/BSSA0710040959**

Bouchon, M. and Coutant, O. (1994). Calculation of synthetic seismograms in a laterally varying medium by the boundary element-discrete wavenumber method. *Bulletin of the Seismological Society of America*, 84(6): 1869–1881. doi: **https://doi.org/10.1785/BSSA0840061869**

Campillo, M., Singh, S. K., Shapiro, N., Pacheco, J., & Hemnann, R. B. (1996). Crustal structure south of the Mexican volcanic belt, base don group velocity dispersion. *Geofísica Internacional*, 35(4), 361–370; **https://doi.org/10.22201/igeof.00167169p.1996.35.4.529**

Campos-Enríquez, J. O., Lermo-Samaniego, J. F., Antayhua-Vera, T., Chavacán, M., and Ramón-Márquez, V.-M. (2015). The Aztlán Fault System: control on the emplacement of the Chichinautzin Range volcanism, southern Mexico Basin, Mexico. Seismic and gravity characterization. *Boletín de la Sociedad Geológica Mexicana*, 67(2), 315-335. doi: **http://dx.doi.org/10.18268/BSGM2015v67n2a13**

Coutant, O. (1989). Numerical study of the diffraction of elastic waves by fluid-filled cracks. *Journal of Geophysical Research*, 94(B12). doi: **https://doi.org/10.1029/JB094IB12P17805**

Cruz-Atienza, V. M., Iglesias, A., Pacheco, J. F., Shapiro, N. M., and Singh, S. K. (2010). Crustal structure below the valley of Mexico estimated from receiver functions. *Bulletin of the Seismological Society of America*, 100(6), 3304–3311. doi: **https://doi.org/10.1785/0120100051**

De Cserna, Z., De la Fuente-Duch, M., Palacios-Nieto, M., Triay, L., Mitre- Salazar, L. M., and Mota-Palomino, R. (1987). Estructura Geológica, Gravimétrica, Sismicidad y relaciones Neotectónicas Regionales de la Cuenca de México. *Boletín Instituto de Geología.* Universidad Nacional Autónoma de México. 104.

Delvaux, D., and Barth, A. (2010). African stress pattern from formal inversion of focal mechanism data. *Tectonophysics*, 482(1–4), 105–128. doi: **https://doi.org/10.1016/j.tecto.2009.05.009**

Delvaux, D., and Sperner, B. (2003). New aspects of tectonic stress inversion with reference to the TENSOR program. *Geological Society London Special Publications*, 212(1):75-100. doi: **https://doi.org/10.1144/GSL.SP.2003.212.01.06**

Ego F. and V. Ansan, (2002). Why is the Central Trans-Mexican Volcanic Belt (102°–99°W) in transtensive deformation?, *Tectonophysics* 359(1-2), 189–208. doi: **https://doi.org/10.1016/S0040-1951(02)00511-5**

Espíndola, V. H., Quintanar, L., and Espíndola, J. M. (2017). Crustal structure beneath Mexico from receiver functions. *Bulletin of the Seismological Society of America*, 107(5), 2427–2442. doi: **https://doi.org/10.1785/0120160152**

Ferrari, L., Orozco-Esquivel, T., Manea, V. (2012). The dynamic history of the Trans-Mexican Volcanic Belt and the Mexico subduction zone. *Tectonophysics*, 522, 122-149. doi: **https://doi.org/10.1016/j.tecto.2011.09.018**

Figueroa, J. (1971). Sismicidad en la Cuenca del Valle de México, Serie de Investigación, 289, *Instituto de Ingeniería*, UNAM, México.

Flores López R., (1987); Informe geológico final del estudio sísmico de reflexión de la Ciudad de México, México, PEMEX.

García Acosta, V., Suárez, G. (1996). Los sismos en la historia de México: *El análisis social. Universidad Nacional Autónoma de México, Centro de Investigaciones y Estudios Superiores en Antropología Social.* Fondo de Cultura Económica.

García-Palomo, Armando, Zamorano, José Juan, López-Miguel, Celia, Galván-García, Adriana, Carlos-Valerio, Víctor, Ortega, Roberto, & Macías, José Luis. (2008). El arreglo morfoestructural de la Sierra de Las Cruces, México central. *Revista mexicana de ciencias geológicas*, 25(1), 158-178.

Gómez-Tuena, A., Orozco-Esquivel, M., and Ferrari, L. (2007). Igneous petrogenesis of the Trans-Mexican volcanic belt. *Boletín de la Sociedad Geológica Mexicana*, 57(3), 227-283. doi: **https://doi.org/10.18268/bsgm2005v57n3a2**

Havskov J. (1982). The Earthquake Swarm of February 1981 in Mexico City, *Geofísica Internacional*. 21(2), 157-175. doi: **https://doi.org/10.22201/igeof.00167169p.1982.21.2.909**

Havskov, J. and S. K. Singh (1978). Shallow crustal structure below Mexico City, *Geofísica Internacional*. 17(2), 223-229. doi: **https://doi.org/10.22201/igeof.00167169p.1978.17.2.935**

Havskov, J., Voss, P. H., and Ottemöller, L. (2020). Seismological observatory software: 30 yr of Seisan. *Seismological Research Letters*, 91(3), 1846–1852. doi: **https://doi.org/10.1785/0220190313**

Heidbach, O., Tingay, M., Barth, A., Reinecker, J., Kurfeß, D., and Müller, B. (2010). Global crustal stress pattern based on the World Stress Map database release 2008. *Tectonophysics*, 482(1–4), 3–15. doi: **https://doi.org/10.1016/j.tecto.2009.07.023**

Kagan, Y. Y. (1991). 3-D rotation of double-couple earthquake sources. *Geophysical Journal International*, 106(3), 709–716. doi: **https://doi.org/10.1111/j.1365-246X.1991.tb06343.x**

Kikuchi, M. and Kanamori, H. (1991). Inversion of complex body waves—III. *Bulletin of the Seismological Society of America*, 81(6): 2335–2350. doi: **https://doi.org/10.1785/BSSA0810062335**

Lugo-Hubp, J., Mooser, F., Pérez- Vega, A., and Zamorano-Orozco, J. (2019). Geomorphology of the Sierra of Santa Catarina, D.F., Mexico. *Revista Mexicana De Ciencias Geológicas*, 11(1), 43–52.

Macías, J. L., Arce, J. L., García-Tenorio, F., Layer, P. W., Rueda, H., Reyes-Agustin, G., López-Pizaña, F., and Avellán, D. (2012). Geology and geochronology of Tlaloc, Telapón, Iztaccíhuatl, and Popocatépetl volcanoes, Sierra Nevada, central Mexico. *GSA Field Guides*, 25, 163–193. doi: **https://doi.org/10.1130/2012.0025(08)**

Manzanilla, L. (1986). Relación de los sismos ocurridos en la ciudad de México y sus efectos. Sismo: Desastre y Sociedad en la Ciudad de México. *Revista Mexicana de Sociología*. 48(2), 265-282. doi: **https://doi.org/10.2307/3540365**

Márquez, A., Verma S., Anguita F., Oyarzun, R., Brandle, J.L. (1999). Tectonics and volcanism of Sierra Chichinautzin: Extension at the front of the Central Trans-Mexican Volcanic belt. *Journal of Volcanology and Geothermal Research*, 93, 125-150. doi: **https://doi.org/10.1016/S0377-0273(99)00085-2**

Marsal, R, and R. Graue, (1969); *El subsuelo del lago Texcoco, el hundimiento de la Ciudad de México y proyecto Texcoco (Nabor Carrillo).* Secretaria de Hacienda y Crédito Público, México

Mooser, F., Montiel, A., Zúñiga, Á. (1992). El suroeste de la cuenca de México en el nuevo mapa geológico. Experiencias geotécnicas en la zona poniente del Valle de México. México: *Sociedad Mexicana de Mecánica de Suelos*, 5–16.

PEMEX, (1986); *Estudio geológico de México*.

Pérez Cruz, G. A. (1988). *Estudio sismológico de reflexión del subsuelo de la Ciudad de México.* [Tesis de Maestría, Universidad Nacional Autónoma de México] Repositorio de Tesis DGBSDI **https://ru.dgb.unam.mx/handle/20.500.14330/TES01000074449.**

Pérez-Campos, X., Y. Kim, A. Husker, P. M. Davis, R. W. Clayton, A. Iglesias, J. F. Pacheco, S. K. Singh, V. C. Manea, and M. Gurnis (2008), Horizontal subduction and truncation of the Cocos Plate beneath central Mexico, *Geophysical Research Letters*, 35(18). doi: **https://doi.org/10.1029/2008GL035127.**

Quintanar, L. Singh, S. K., Espíndola, V. H., Iglesias, A., Bello-Segura, D. I., Arroyo, D. (2024) Mexico City Earthquake of 11 May 2023 (Mw3.2). *Geofísica Internacional*. 63-2: 749–762. doi: **https://doi.org/10.22201/igeof.2954436xe.2024.63.2.1757**

Quintanar, L., Cárdenas-Ramírez, A., Bello-Segura, D. I., Espíndola, V. H., Pérez-Santana, J. A., Cárdenas-Monroy, C., Carmona-Gallegos, A. L., and Rodríguez-Rasilla, I. (2018). A Seismic Network for the Valley of Mexico: Present Status and Perspectives. *Seismological Research Letters, 89(2A)*, 356–362. doi: **https://doi.org/10.1785/0220170198.**

Siebe, C., and Macías, J. L. (2004). Volcanic hazards in the Mexico City metropolitan area from eruptions at Popocatépetl, Nevado de Toluca, and Jocotitlán stratovolcanoes and monogenetic scoria in the Sierra Chichinautzin Volcanic Field. En A. Claus Siebe, José Luis MacíasGerardo, J. Aguirre-Díaz (Eds.). *Neogene-Quaternary Continental Margin Volcanism: A perspective from México* (pp. 253-329). Geological Society of America doi: **https://doi.org/10.1130/2004.VHITMC.SP402**

Singh, S. K, Quintanar-Robles, L., Arroyo, D., Cruz-Atienza, V. M., Espíndola, V. H., Bello-Segura, D. I., and Ordaz, M. (2020). Lessons from a Small Local Earthquake (M w 3.2) That Produced the Highest Acceleration Ever Recorded in Mexico City. *Seismological Society of America, 91(6)*, 3391-3406. doi: **https://doi.org/10.1785/0220200123**

Singh, S. K., Lermo, J., Dominguez, T., Ordaz, M., Espinosa, J. M., Mena, E., and Quaas, R. (1988a). The Mexico Earthquake of September 19, 1985—A Study of Amplification of Seismic Waves in the Valley of Mexico with Respect to a Hill Zone Site. *Earthquake Spectra* 4(4), 653–673. doi: **https://doi.org/10.1193/1.1585496**

Singh, S. K., Mena, E., and Castro, R. (1988b). Some aspects of source characteristics of the 19 September 1985 Michoacan earthquake and ground motion amplification in and near Mexico City from strong motion data. *Bulletin of the Seismological Society of America*, 78(2), 451–477. doi: **https://doi.org/10.1785/BSSA0780020451**

Singh, S. K., Ordaz, M., Pacheco, J. F., and Courboulex, F. (2000). A simple source inversion scheme for displacement seismograms recorded at short distances. *Journal of Seismology*, 4, 267–284. doi: **https://doi.org/10.1023/A:1009849819475**

Sokos, E. and Zahradnik, J. (2008). ISOLA-A Fortran code and Matlab GUI to perform multiple point source inversion of seismic data. *Computers and Geosciences*. 34. 967-977. doi: **https://doi.org/10.1016/j.cageo.2007.07.005**

Sokos, E., and Zahradník, J. (2013). Evaluating centroid-moment-tensor uncertainty in the new version of ISOLA software. *Seismological Research Letters*, 84(4), 656–665. doi: **https://doi.org/10.1785/0220130002**

UNAM and CENAPRED Seismology Group (1995). The Milpa Alta earthquake of January 21, 1995. *Geofísica Internacional*, 34(4), 355–362. doi: **https://doi.org/10.22201/igeof.00167169p.1995.34.4.1420**